7

Modeling of Growth of High-k Oxides on Semiconductors

C.J. Först, C.A. Ashman, K. Schwarz, and P.E. Blöchl

Summary. The replacement of SiO_2 by so-called high-k oxides is one of the major challenges for the semiconductor industry to date. Based on electronic structure calculations and ab initio molecular dynamics simulations, we are able to provide a consistent picture of the growth process of a class of epitaxial oxides around SrO and $SrTiO_3$. To the best of our knowledge this is the only theoretical study which considers the whole growth process starting from the clean Si substrate. Knowledge of the initial growth steps such as metal adsorption on the Si surface has proven to be vital for the understanding of the growth process. The knowledge of the interfacial binding principles has also allowed us to propose a way to engineer the band-offsets between the oxide and the silicon substrate. The results obtained for the Si substrate are directly transferable to Ge.

7.1 Introduction

The replacement of SiO_2 as a gate dielectric in microelectronic devices is one of the key challenges of the semiconductor industry in the next years [1]. Due to their larger dielectric constants, so-called high-k oxides can be deposited with greater physical thicknesses which reduces the quantum-mechanical leakage currents through insulating oxide layers. The growth of these, mostly transition metal containing oxides on the technologically relevant Si(001) surface has proven to be highly challenging. While in a first phase amorphous oxides, based on ZrO_2 or HfO_2 in connection with an ultra-thin SiO_2 layer, will be employed, industry requires solutions for crystalline oxides with an epitaxial interface to the silicon substrate as soon as 2013 [1]. However, there is only one clear demonstration of an atomically well-defined interface between silicon and a high-k oxide so far, namely $SrTiO_3$. Despite the clear experimental evidence of an atomically well-defined interface [2], the interfacial stoichiometry and structure have remained elusive until recently. Key process parameters as well as the electronic properties at the interface are still under debate. Using ab initio molecular dynamics simulations we have been able to unravel the growth process of $SrTiO_3$ on Si(001) and propose a way to engineer the

band offsets with respect to silicon [3, 4]. The detailed understanding of the chemistry of group II–IVa transition metals on the silicon(001) surface has proven to be vital in order to rationalize the mechanisms of interface formation. Recent results show that the basic binding principles can also be applied to investigate the interfacial chemistry between silicon and $LaAlO_3$ [5]. This chapter summarizes the results obtained by the authors in this context. In depth information can be found in our previous publications [3–7]. Other theoretical studies on $SrTiO_3$ can be found in [8–10]. We will concentrate on our work since it provides a consistent picture of the growth process from the clean silicon surface to the first few monolayers of the oxide film.

7.2 Computational Approach

Simulations close the gap between analytical theory as well as experiment and constitute a third field of modern materials research. They allow the exploration of models which cannot be solved analytically and therefore contain fewer approximations. Atomistic simulations give information about the position and momentum of individual atoms in molecules, on surfaces or in bulk materials and allow the calculation of the electronic structure. Computational materials scientists can furthermore perform computer experiments under any imaginable condition or stoichiometry, which enables them to explore situations that are not accessible experimentally. For example, knowledge about transitions states is crucial for the understanding of chemical processes but, due to their short life-times, they may not be easily detectable via experiment. However, it is possible to accurately determine transition states computationally. Computational simulation is a rather new and novel field in materials science. The first approaches towards simulation were done during World War II in the context of the Manhattan project. The limited computer capabilities in previous decades and also the nonavailability of reliable models and efficient numerical techniques was responsible that it took several decades until computer simulations became "everyday business."

The basis of every simulation is a reliable model that is a simplified description of the real system. Such models can provide us for example with the total energy as a function of atomic configurations, and maybe also other parameters such as volume, temperature or electronic structure. The proper physical framework in microscopic systems is quantum mechanics. So-called ab initio or first principles models are purely based on the theorems of quantum mechanics and do not require any experimental input parameters other than the chemical composition and charge state of the system. Since for systems of interest it is impossible to solve the Schrödinger equations exactly, approximations have to be made.

The results presented here are based on density functional theory [11, 12], an efficient method to calculate the ground state energies from first principles which has become state-of-the-art in computational materials science. We use

the projector augmented wave method [13, 14] to represent wave-functions and densities. The trajectories of the atoms are computed using the ab initio molecular dynamics scheme [15]. All calculations were done on a five layer-model of the (001) surface of the silicon substrate where the bottom layer was saturated with hydrogen and frozen at bulk positions. Further details about the computational procedure can be found in our previous publications in this field [3–7].

7.3 The Chemistry of the Substrate

Silicon crystallizes in the diamond structure. Each atom is tetrahedrally coordinated and forms four covalent bonds. Cleaving the crystal along a (001) plane creates a surface with a quadratic (1 × 1) array of silicon atoms (compare Fig. 7.1a). Each surface atom exhibits two partially occupied dangling bonds pointing out of the surface. This situation is energetically highly unfavorable and leads to the (4 × 2) buckled dimer row reconstruction of the silicon (001) surface. We will shortly review its atomic and electronic structure, since it is a key to understand the oxide growth: In a first reconstruction step, two neighboring silicon atoms approach each other and form the so-called dimer bond which is parallel to the surface. The result is the (2 × 1) dimer row reconstructed silicon surface which leaves only one singly occupied dangling bond state per surface silicon atom (compare Fig. 7.1b). The bonding and anti-bonding states of the dimer bonds move out of the gap into the valence and conduction band, respectively.

The half-filled dangling bond band is then, in a second step, split into two subands, one fully occupied the other empty. The reason for this lift in degeneracy is a geometrical distortion, namely the tilt of the dimer bond. One silicon atom moves up and adopts a quasi-tetrahedral, sp^3-like bonding arrangement, the other one moves down and ends up in a planar, sp^2-like bonding environment. This process is called "buckling." Along one dimer row, the buckling is strongly correlated in an anti-parallel manner. Across the rows, the correlation is comparably weak. This second step results in the final $c(4 \times 2)$ reconstruction of the silicon surface (compare Fig. 7.1c). The fully occupied sub-band is formed by the sp^3-orbitals of the upper silicon atoms and the empty subband with p_z character by the lower silicon atoms. The upper silicon

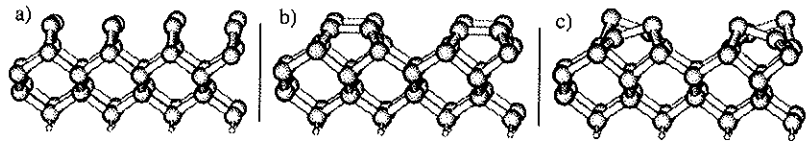

Fig. 7.1. The reconstruction of the Si(001) surface. Panel (**a**): the unreconstructed (1 × 1) surface; panel (**b**): the (2 × 1) reconstruction; panel (**c**): the (4 × 2) reconstruction

atoms are thus formally charged "−1" and the lower silicon atoms "+1." It is important to note that, despite this reconstruction processes, the silicon surface is still considered to be a highly reactive surface. The presence of oxygen or transition metals leads to oxidation and silicidation even at ambient conditions.

7.4 Metal Adsorption on Si(001)

In order to maintain the integrity of the substrate, it is important to avoid the oxidation of silicon. Therefore it is mandatory to start the growth process with the deposition of the metal, an approach followed by most experimental groups. The critical part during growth of an oxide with molecular beam epitaxy (MBE) is the deposition of the metal and the oxidation of the adsorbed metal layers. Therefore a detailed understanding of the adsorption of the metal layer is important to guide the growth process. We have investigated the deposition of metal ions selected from the three most relevant groups in the context of high-k oxides on the silicon(001) surface [16, 17]. These are the divalent earth-alkali metals and the three- and four-valent transition metals exemplified by strontium $(Sr)^3$, lanthanum $(La)^7$, and zirconium $(Zr)^6$.

We simulated a wide range of adsorbed metal layers and scanned the relevant phase space, which is a considerable task. The search was guided by chemical insight, geometric classification and ab initio simulations that provide an unbiased exploration of a small region of the phase space. While this approach cannot exclude, with certainty, that a particular low-energy structure has been missed, the use of a mixture of various search strategies and a sufficiently wide search space seems to yield fairly reliable results.

Figure 7.2 shows the results for Sr adsorption on silicon. The symbols mark the adsorption energies normalized per (1×1) silicon surface cell as function of coverage in monolayers (represented by appropriate supercells). The adsorption energies are obtained relative to a reservoir of bulk silicon and the most stable silicide, in this case $SrSi_2$. Only the lower envelope is physically relevant. At coverages where the line segments meet we predict stable phases. The slopes of the two line segments correspond to the chemical potentials of the phase boundaries. Figure 7.3 shows the phase diagram as a function of the Sr chemical potential derived from Fig. 7.2. The chemical potential can be related to experimental parameters like partial pressure and temperature. The straight line segments indicate coexistence of the two adjacent stable phases. As the coverage increases within one of the line segments, the surface area of the low-coverage phase is converted into that of the high-coverage phase. Thus we are able to predict the sequence of stable phases at zero temperature. From simple thermodynamic considerations we expect that the qualitative features will not change at finite, but not too high temperatures.

One of the main problems during growth of high-k oxides is the formation of silicide grains. Bulk thermodynamic stability of the relevant metals has

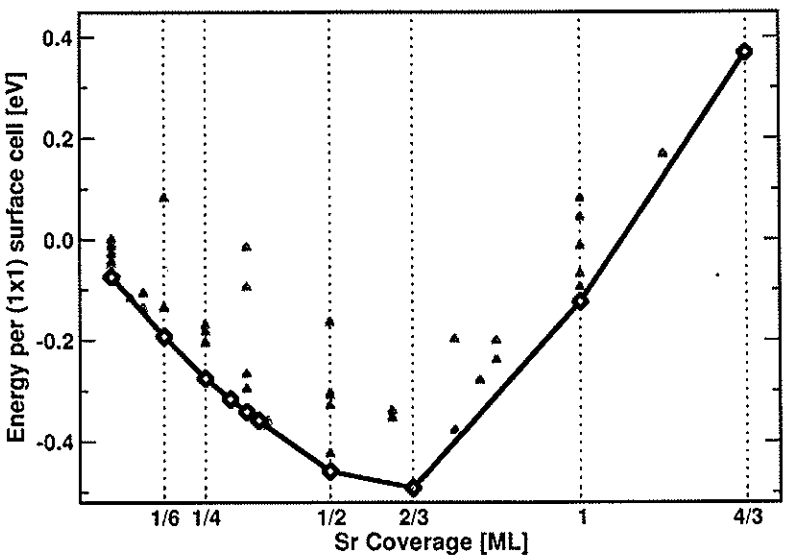

Fig. 7.2. Surface energy vs. coverage for Sr. The *open diamonds* represent thermodynamically accessible structures, the *triangles* correspond to metastable structures

been investigated by Schlom and co-workers [16, 17] but may be misleading for film growth in the monolayer range, since it neglects the effects of epitaxial strain and does not account for the binding of the metal ad-atom layer to the substrate. Going one step further is to compare the energies of the adsorbed metal layer with that of a bulk silicide. Since the adsorption energies have

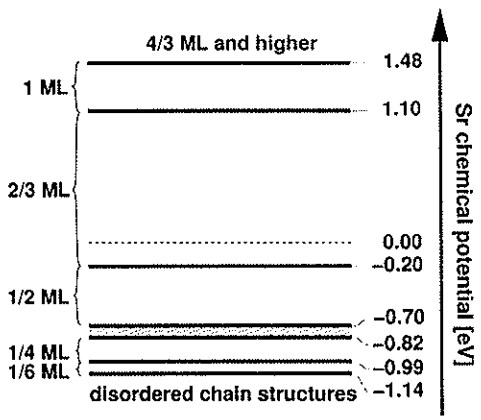

Fig. 7.3. Adsorption phase diagram of Sr on the Si(001) surface as a function of the Sr chemical potential for coverages up to 4/3 ML. For chemical potentials above zero, bulk silicide formation is thermodynamically favorable. The *shaded* region between the 1/4 and 1/2 ML phases indicates disordered surface structures

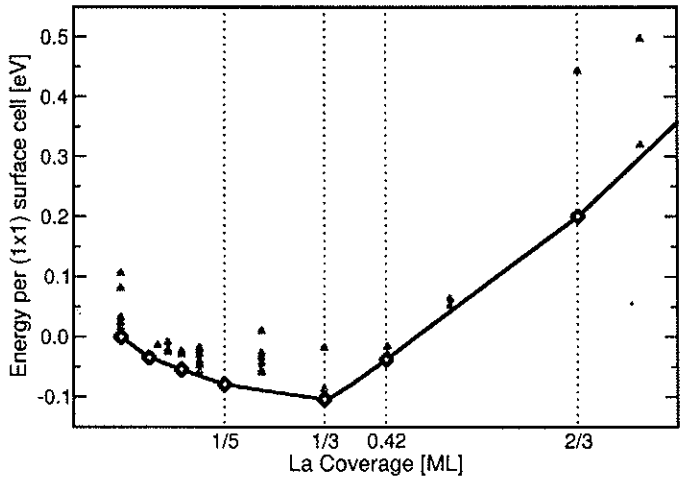

Fig. 7.4. Surface energy vs. coverage for La. The *open diamonds* represent thermodynamically accessible structures, the *triangles* correspond to metastable structures

been calculated with respect to the silicide as a particle reservoir, we obtain the stability limit, where the lower envelope in Fig. 7.2 changes its slope to positive values. Choosing another reservoir would change the slopes of the straight lines, however, the thermodynamically stable reconstructions (i.e., the nodes of the lower envelope) remain the same.

In the case of Sr (compare Fig. 7.2 and 7.3) we calculate coverages up to 2/3 monolayer (ML) as thermodynamically stable [3], whereas for the La surface we find reconstructions only to be stable up to the coverage of 1/3 ML [7] (compare Fig. 7.4). In case of Zr and Hf, all surface reconstructions are unstable with respect to silicide formation, which excludes the possibility of metal pre-deposition [6]. In the case of Zr, we find that the adsorption structures become more stable with increasing coverage indicating that the silicide grows spontaneously. In addition we directly observed the onset of silicide formation in the form of Zr atoms migrating below the Si surface. Zr-silicide formation has also been identified experimentally [18].

The stable surface reconstructions found for Sr and La are driven by the atomic and electronic topology of the Si(001) surface. Here we will summarize the basic principle with the example of Sr. La behaves conceptually similar at low coverages and, due to a change in oxidation state from 3+ to 2+ above 1/3 ML, even identical to Sr at high coverages [7].

The chemistry of Si and Sr is probably best understood in terms of the Zintl–Klemm concept [19–21]. It explains in a simple ionic picture the relationship between stoichiometry and structure for a wide range of compounds between electronegative elements, essentially groups IV–VII, and electropositive elements, mainly groups I and II. The electropositive element, in our example Sr, donates its electrons to the electronegative element, which will

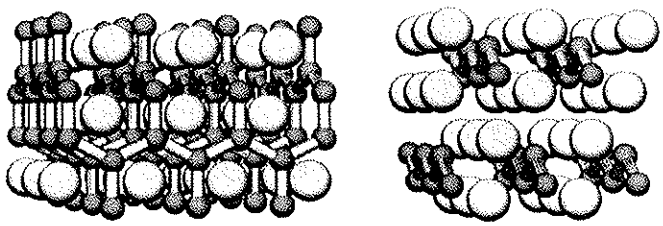

Fig. 7.5. Two typical bulk Sr silicides: $SrSi_2$ (*left*) and SrSi (*right*). Si atoms are visualized by the small spheres connected by sticks and Sr by the big spheres

be Si in this context. Each electron of the electropositive element can saturate one partially filled dangling bond of the electronegative element. As a result the electronegative element forms structures which have a smaller number of covalent bonds. Si^0 forms four bonds, Si^{1-} forms three bonds, Si^{2-} forms two bonds, and so on. The bonding behavior corresponds to a shift to the right in the periodic table of elements for each electron Si receives. Si^-, Si^{2-}, Si^{3-} and Si^{4-} are thus found to be isosteric to P, S, Cl and Ar.

For the example of two bulk Sr silicides shown in Fig. 7.5 we can demonstrate that this simple concept is indeed a useful tool to rationalize the chemistry between Sr and Si. In the left panel we observe that each Si atom forms three covalent bonds. This leaves one valency per Si atom which has to be saturated via electron donation from Sr. Since Sr can donate two valence electrons, the final stoichiometry, according to Zintl–Klemm, must be $SrSi_2$ ($Sr^{2+}Si_2^-$), which is indeed correct. In the example given in the right panel of Fig. 7.5, each Si atom forms two covalent bonds which correspond to two valences that need to be saturated via electron donation or, in other words, formal Si^{2-} ions. The stoichiometry is indeed SrSi ($Sr^{2+}Si^{2-}$). Furthermore, SrSi with its chain structures is a nice example showing that Si^{2-} is isosteric to sulfur which is known for forming chain structures.

Translating the Zintl–Klemm concept to the silicon(001) surface implies that each Sr ad-atom will saturate the dangling bonds of one silicon dimer with its two valence electrons. A saturated dimer looses its buckling, since all dangling bonds are filled and both Si atoms prefer the tetrahedral sp^3 configuration. The atomic structure around an isolated Sr-ad-atom is schematically shown in Fig. 7.6. The preferred adsorption site is in the center of four dimers. One of the neighboring Si dimers is unbuckled due to the electron donation from the ad-atom. The other three dimers are orientated such that the upper, and thus negatively charged Si atom points towards the Sr^{2+} ion. The energy penalty for placing a lower and thus positively charged silicon atom next to an Sr ad-atom is roughly 0.4 eV. Therefore the ad-atoms pin the dimer buckling as observed experimentally [22].

The filled dimer offers a preferred adsorption site in the next valley as indicated by the open circle in Fig. 7.6. As a result, diagonal and zig-zag chain structures turn out to be the thermodynamically stable reconstructions

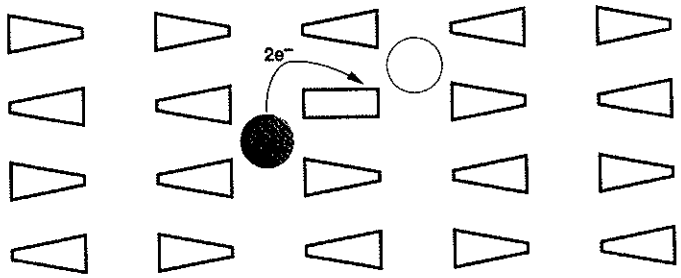

Fig. 7.6. Schematic representation of the isolated Sr ad-atom at the preferred adsorption site position. The *filled circle* represents the Sr ad-atom, the *rectangle* represents a filled and therefore unbuckled Si dimer. The *triangles* represent buckled dimers. The *flat side* of a buckled dimer indicates the upper Si atom with a filled dangling bond, whereas the pointed side indicates the lower Si atom with the empty dangling bond. The charge transfer from the Sr ad-atom to one of the surrounding dimers is indicated by the *arrow*, the preferred adsorption site in the neighboring valley by the *open circle*

at low coverages. At 1/6 ML these chains condense (compare left panel of Fig. 7.7). It is not possible to stack them with a separation of only two instead of three dimer spacings because that would imply that a lower and thus positively charged Si atom points towards an Sr ion which involves a large energy penalty as discussed above. This is the reason for a distinct phase at a coverage of 1/6th ML (compare phase diagram in Fig. 7.3). The next stable phase is made of double chains at 1/4 ML as shown in the right panel of Fig. 7.7. Chain structures at low coverages have also been observed experimentally [23–25].

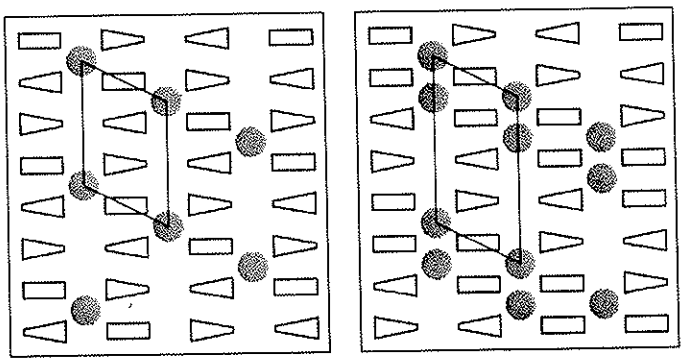

Fig. 7.7. Chain structures of Sr ad-atoms at low coverages. The symbols are explained in Fig. 7.6. The surface unit cells are outlined. *Left*: Condensed diagonal chains of Sr at a coverage at 1/6 ML. *Right*: Diagonal double chains of Sr at a coverage of 1/4 ML

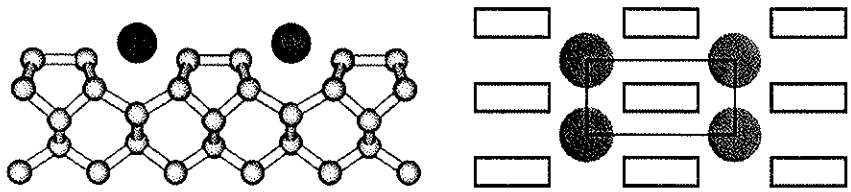

Fig. 7.8. The (2 × 1) reconstruction at a coverage of 1/2 monolayer. *Left panel*: ball-stick model; *right panel*: schematic top-view

The phases at 1/6 ML and at 1/4 ML correspond to those observed by McKee et al. by their (1 × 3) and (1 × 2) RHEED pattern [18]. The presence of these phases has been one main argument for proposing a solid-state transformation to a silicide phase as expected from the bulk phase diagram. However, our calculations clearly show that the structural model proposed by McKee [26] is higher in energy than the structures discussed above. Therefore, we rule out the model of a transformation into a silicide layer of the form proposed by McKee et al. [2] for clean substrates.

At one half monolayer, the Sr ad-atoms occupy all favorable positions in the center of four dimers (compare Fig. 7.8). We labeled this coverage as the "canonical coverage" because all dangling bond states are saturated. Consequently we find that there are no surface states deep in the gap of silicon. This surface is isoelectronic to a hydrogen terminated silicon surface and thus is expected to be chemically comparably inert. Experimentally it has been found that the surface is exceptionally inert against oxidation at 1/2 ML of Sr [27].

Above 1/2 ML, the electrons donated by Sr ad-atoms enter the dimer antibonding states leading to a partial breakup of the dimer bonds. At 2/3 ML we observe a (3 × 1) reconstruction with alternating rows of Si dimers and isolated Si atoms as depicted in Fig. 7.9. All reconstructions above this coverage are thermodynamically unstable against bulk silicide formation.

Lanthanum adsorption follows similar principles with two main differences [7]: Firstly, La donates three electrons instead of two. This changes the phase-diagram considerably, despite very similar building principles (Fig. 7.10 shows the double-stepped La rows at 1/6 ML as compared to the single-stepped Sr rows shown in Fig. 7.7). Secondly, La deviates from the Zintl–Klemm concept in that it changes its charge state from being a formal La^{3+} ion at lower coverages to a La^{2+} ion at coverages above 1/3 ML. However, the structures above 1/3 ML are no more thermodyamically stable against the formation of La silicide. Note however, that these predictions do not exclude the formation of metastable layers beyond a coverage of 1/3 ML.

These studies of the adsorption of two-, three-, and four-valent metals on Si(001) have led to a unified picture of the processes and have added new insight that allows to explain a number of experimental data. The results furthermore have led to the discovery of the interface structure between silicon and $SrTiO_3$.

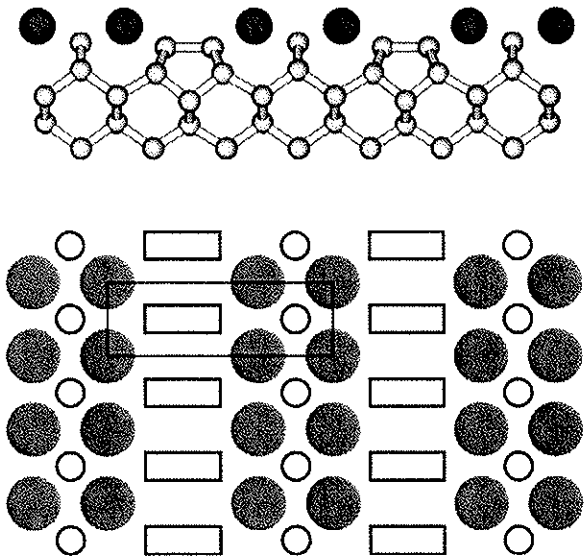

Fig. 7.9. The (3 × 1) reconstruction at an Sr coverage of 2/3 ML. *Top panel*: ball-stick model; *bottom panel*: schematic top-view

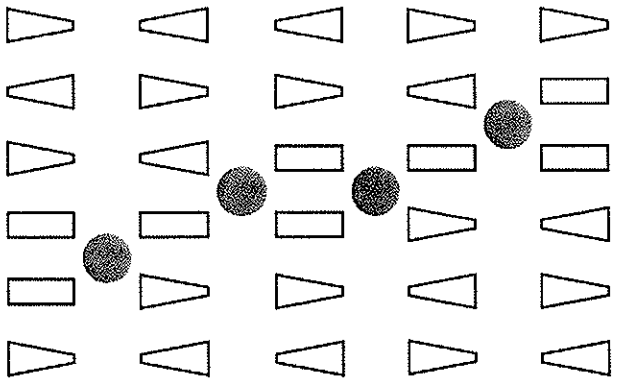

Fig. 7.10. Single La chain on the silicon substrate. Due to the different electron count (La donates three valence electrons to the substrate) we predict double-stepped chains

7.5 Interface of $SrTiO_3$ and Si(001)

The chemical bonding in silicon and $SrTiO_3$ is fundamentally different. While silicon is a covalently bonded material, $SrTiO_3$ is an ionic crystal with some covalent character in the Ti–O bonds. More specifically, $SrTiO_3$ crystallizes in the perovskite structure with Ti being octahedrally coordinated by oxygen and Sr placed in a cubic oxygen cage. The (001) planes of $SrTiO_3$ are

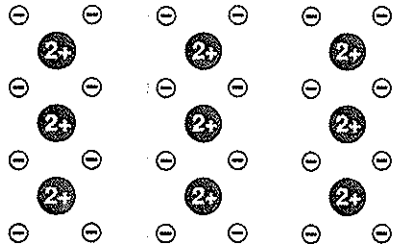

Fig. 7.11. Charge pattern of the silicon surface covered by 1/2 ML of Sr. The Sr ions have a formal charge of 2+, Si of 1− due to the filled dangling bond. The empty *rectangles* denote the dimer bonds, that are included to relate this figure with the lower left panel of Fig. 7.12

alternating SrO and TiO_2 planes that are electronically saturated ($Ti^{4+}O_2^{2-}$ and $Sr^{2+}O^{2-}$) and thus are unable to form covalent bonds. The SrO terminated surface does not exhibit states in the band gap. An electronically saturated Si–$SrTiO_3$ stack must thus exhibit an interfacial layer which provides a covalent bonding environment towards the silicon substrate and in addition an ionic template compatible with that of $SrTiO_3$. The only Sr covered surface meeting these requirements is the reconstruction at 1/2 ML. It is the only one which saturates all silicon dangling bonds and does not have surface states in the band-gap of silicon. The quasi-ionic interaction of Sr with Si furthermore prepares an ionic template with a formal charge distribution as visualized in Fig. 7.11. The resulting two-dimensional ionic layer is compatible with the NaCl-type charge pattern of an SrO-terminated $SrTiO_3$ crystal.

We started from this Sr-passivated substrate and simulated the deposition of one layer of SrO. During a heating cycle to 600 K this single oxide layer reconstructs significantly. However, after placing two or more layers of SrO or $SrTiO_3$ on top of the reconstructed SrO layer, the oxide layers crystallize into the perfect bulk structure. Thus we obtain an atomically abrupt interface between the silicon substrate and the high-k oxide. This interface structure, denoted A and shown in Fig. 7.12, corresponds to the Sr-passivated silicon surface matched to the nonpolar SrO layer of the oxide. It emerged as the only possible candidate for an electronically saturated interface structure. Furthermore it is compatible with all unambiguous features of the Z-contrast image of McKee et al. [2] Similar structures can also be formed by directly growing $SrTiO_3$ with the TiO_2 layer in direct contact with the Sr-covered Si surface.

7.6 Band Offset Engineering

An electrically inactive interface is only one of the requirements a high-k oxide has to meet. A common problem with high-k oxides is a conduction-band offset between silicon and the oxide which is too small. This offset acts as an electron injection barrier, which prevents electrons from being drawn

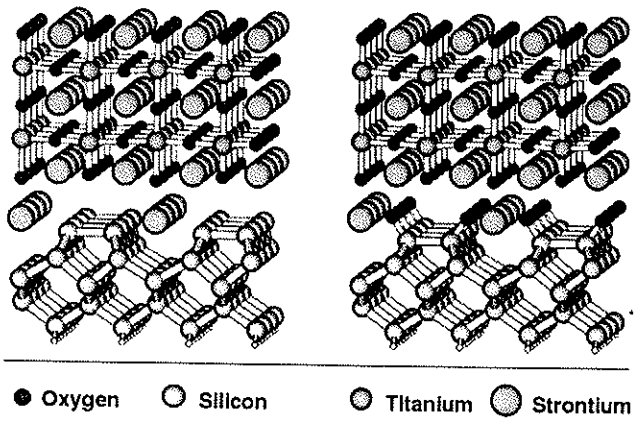

Fig. 7.12. The two relevant interface structures between silicon and $SrTiO_3$. *Left panel*: interface structure A with an Sr-passivated Si surface; *right panel*: interface structure B with oxidized dangling bonds

into the gate from the channel via the gate-oxide. For device applications, the conduction and valence band offsets have to be in the range of 1 eV or larger. However, for the interface just introduced (left panel of Fig. 7.12) we calculate a conduction band offset of only 0.2 eV, which is in line with measurements done on related interfaces [28].

Depending on growth and annealing conditions, the oxygen content of the interface can change. Oxygen can be introduced during growth, or it can diffuse in from the oxide. Therefore it is important to investigate the stability of the interface against oxidation [4]. We find that oxygen first attacks the filled dangling bonds of the silicon dimer atoms. In this way exactly one monolayer of oxygen can be selectively introduced at the interface. The resulting interface structure is shown in the right panel of Fig. 7.12 and labeled interface B. We confirmed that this interface can be formed without growing an interfacial SiO_2 layer by oxidizing the substrate. The phase diagram for oxygen at the interface is shown in Fig. 7.13. At very low chemical potentials, corresponding to a low oxygen partial pressure, interface A is stable. As the chemical potential is increased, dimer bonds get oxidized (above–0.60 eV). Within the region of interface B (–0.24 to 0.05 eV) all dimers are oxidized. When leaving the stability range of interface B, dimer bonds are transformed into Si–O–Si bridges, a phase which we label "dimer-oxidized interface B."

Interestingly we find that the oxygen monolayer at the interface increases the conduction band offset by 1.1 eV. The resulting injection barrier of 1.3 eV is in line with technological requirements. The origin of this effect is visualized in Fig. 7.14. The additional interface dipole formed by the Si^+ and O^{2-} ions in interface B is responsible for a shift of 1.1 eV in the electrostatic potential within the oxide relative to the silicon substrate. This shift directly translates into a shift of the oxide band structure and thus increases the conduction band offset by the same amount.

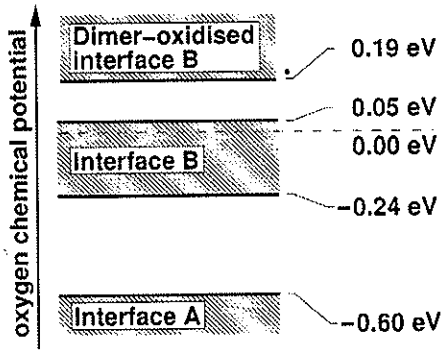

Fig. 7.13. Phase diagram for interface oxidation. *Shaded areas* indicate the stability regions of the defect-free interfaces A and B and the dimer-oxidized variant of interface B. The blank regions separating them correspond to disordered structures with an oxygen content that increases with increasing chemical potential. The external parameter is the oxygen chemical potential. The zero of the chemical potential corresponds to the coexistence of bulk Si and SiO_2 (a-quartz) in thermal equilibrium

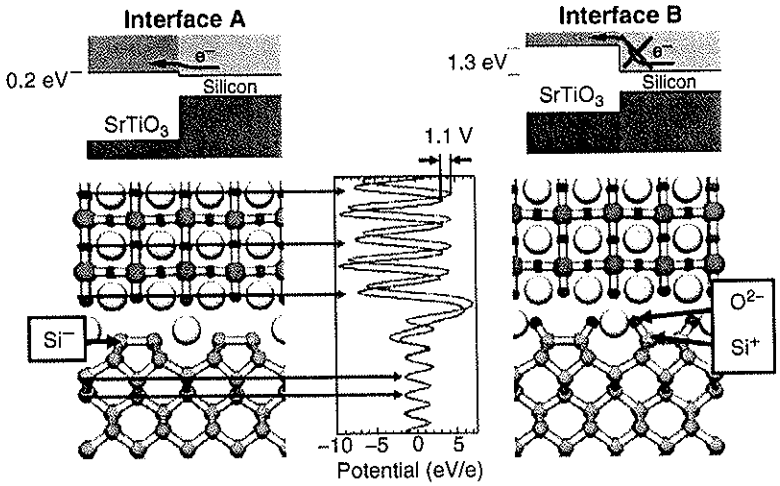

Fig. 7.14. Cause and effect of the interface oxidation. The *top row* shows a schematic drawing of the evolution of the band edges near the interface. The conduction band offset for interface A is only 0.2 eV. The *bottom row* shows interfaces A and B as well as the average electrostatic potential in planes parallel to the interface. The *blue curve* corresponds to interface A, the *red curve* to interface B. The *horizontal arrows* are a guide to the eye and mark the positions of the atomic planes in the potential curve. The relative shift in potential of 1.1 eV is observable and directly translated into a correspondingly increased conduction band offset of interface B (*top right*)

To the best of our knowledge, $SrTiO_3$ is the only high-k oxide, for which a controlled growth of an atomically well-defined interface with silicon has been demonstrated experimentally and theoretically. This system has nearly been discarded from the list of potential high-k oxides because of the small electron injection barrier. Our finding that the band offset may be adjusted by selective oxidation of the interface bears the hope that $SrTiO_3$ can still be made useful for device applications.

7.7 Conclusions

We have summarized the detailed picture of metal adsorption from groups II to IVa on silicon(001) that has emerged from our calculations. We have rationalized the sequence of phases seen during metal adsorption in a simple, intuitive and generalized picture. These simulations have led to a structure model for the interface of $SrTiO_3$ and Si(001), which differs from earlier proposals and is compatible with published experimental results. We furthermore investigated the chemical changes of the interface upon oxidation. We have shown that the electron injection barrier can be dramatically increased by controlled oxidation of the interface, in order to match the technological requirements. It is, however, crucial to first form the $SrTiO_3$/Si interface before the oxidation of the interface is done. Otherwise a too high oxygen pressure in the early stage of the growth process would unavoidable lead to SiO_2 formation that must be prevented.

Acknowledgments

We thank A. Dimoulas, J. Fompeyrine, J.-P. Loquet for useful discussions. Clemens Först acknowledges the support from S. Yip and J. Li. This work has been funded by the European Commission in the project Integration of Very High-K Dielectrics with CMOS Technology ("INVEST"), the European project ET4US "Epitaxial Technologies for Ultimate Scaling" and by the AURORA project of the Austrian Science Fond. Parts of the calculations have been performed on the Computers of the "Norddeutscher Verbund für Hoch- und Höchstleistungsrechnen (HLRN)." This work has benefited from the collaborations within the ESF Program on "Electronic Structure Calculations for Elucidating the Complex Atomistic Behavior of Solids and Surfaces."

References

1. 2003 Edition of the ITRS, http://public.itrs.net/
2. R.A. McKee, F.J. Walker and M.F. Chisholm, Phys. Rev. Lett. **81**, 3014 (1998)
3. C.R. Ashman, C.J. Först, K. Schwarz and P.E. Blöchl, Phys. Rev. B **69**, 75309 (2004)

4. C.J. Först, C.R. Ashman, K. Schwarz and P.E. Blöchl, Nature 427, **53** (2004)
5. C.J. Först, K. Schwarz and P.E. Blöchl, Phys. Rev. Lett **95**, 137602 (2005)
6. C.J. Först, P.E. Blöchl and K. Schwarz, Comp. Mater. Sci **27**, 70 (2003)
7. C.A. Ashman, C.J. Först, K. Schwarz and P.E. Blöchl, Phys. Rev. B **70**, 155330 (2004)
8. X. Zhang, A.A. Demkov, H. Li, X. Hu and Y. Wei, Phys. Rev. B **68**, 125323 (2003)
9. J. Robertson and P.W. Peacock, Mat. Res. Soc. Symp. Proc. 747, **99** (2002)
10. P.W. Peacock and J. Robertson, Appl. Phys. Lett. **83**, 5497 (2003)
11. P. Hohenberg and W. Kohn, Phys. Rev. **136**, B864 (1964)
12. W. Kohn and L.J. Sham, Phys. Rev. **140**, A1133 (1965)
13. P.E. Blöchl, Phys. Rev. B **50**, 17953 (1994)
14. P.E. Blöchl, C.J. Först and J. Schimpl, Bull. Mater. Sci. **26**, 33 (2003)
15. R. Car and M. Parrinello, Phys. Rev. Lett. **55**, 2471 (1985)
16. K.J. Hubbard and D.G. Schlom, J. Mater. Res. **11**, 2757 (1996)
17. D.G. Schlom and J.H. Haeni, MRS Bulletin **27**, 198 (2002)
18. Y.M. Sun et al., Appl. Surf. Sci. **161**, 115 (2000)
19. E. Zintl, Angew. Chem. **52**, 1 (1939)
20. W. Klemm, Proc. Chem. Soc. London, 329 (1958)
21. E. Bussmann, Z. Anorg. Allg. Chem. **313**, 90 (1961)
22. X. Yao et al., Phys. Rev. B**59**, 5115 (1999)
23. R.Z. Bakhtizin, J. Kishimoto, T. Hashizume and T. Sakurai, Appl. Surf. Sci. **94/95**, 478 (1996)
24. R.Z. Bakhtizin, J. Kishimoto, T. Hashizume and T. Sakurai, J. Vac. Sci. Technol. B **14**, 1000 (1996)
25. K. Ojima, M. Yoshimura and K. Ueda, Phys. Rev. B **65**, 075408 (2002)
26. R.A. McKee, F.J. Walker and M.F. Chisholm, Science **293**, 468 (2001)
27. Y. Liang, S. Gan. and M. Engelhard, Appl. Phys. Lett. **79**, 3591 (2001)
28. S.A. Chambers, Y. Liang, Z. Yu, R. Droopad and J. Ramdani, J. Vac. Sci. Technol. A **19**, 934 (2001)

Athanasios Dimoulas
Evgeni Gusev
Paul C. McIntyre
Marc Heyns
Editors

SPRINGER SERIES IN ADVANCED MICROELECTRONICS 27

Advanced Gate Stacks for High-Mobility Semiconductors

Springer

A. Dimoulas E. Gusev
P.C. McIntyre M. Heyns
(Eds.)

Advanced Gate Stacks for High-Mobility Semiconductors

With 292 Figures

Springer

Dr. Athanasios Dimoulas
National Center for Scientific Research
DEMOKRITOS, Patriarchou Grigoriou &
Neapoleos, 15310, Aghia Paraskevi,
Athens, Greece
E-mail: dimoulas@ims.demokritos.gr

Evgeni Gusev
QUALCOMM Inc.
5775 Morehouse Dr., San Diego, CA 92121, USA
QUALCOMM MEMS Technologies
2581 Junction Ave. San Jose, CA 95134, USA
E-mail: egusev@qualcomm.com

Professor Paul C. McIntyre
Stanford University
Department for Materials Science
McCullogh Building, Stanford, CA 94305, USA
E-mail: pcm1@stanford.edu

Professor Marc Heyns
IMEC
Kapeldreef 75
3001 Leuven, Belgium
also at Katholieke Universiteit Leuven,
MTM Department
E-mail: marc.heyns@imec.be

ISSN 1437-0387

ISBN-10 3-540-71490-1 Springer Berlin Heidelberg New York
ISBN-13 978-3-540-71490-3 Springer Berlin Heidelberg New York

Library of Congress Control Number: 2007931596

Camera-ready by the Author and SPi, Pondicherry
Cover: eStudio Calmar Steinen

Printed on acid-free paper SPIN: 12029037 57/3180/SPi - 5 4 3 2 1 0